Pre- and Post-rehabilitation Monitoring of a Steel Railway Bridge with Distributed and Discrete Sensors

Christian Barker[1], Joshua Woods[2], A.M.ASCE Neil A. Hoult, M.ASCE[3], Hoat Le, P.Eng.[4], and Vamsi Tolikonda, P.Eng.[5]

[1]Researcher, Department of Civil Engineering, Queen's University, Ellis Hall, Kingston, ON K7L 3N6, Canada. E-mail: christian.john.barker@gmail.com
[2]Mitchell Professor in Intelligent Infrastructure Monitoring. Department of Civil Engineering, Queen's University, Ellis Hall, Kingston, ON K7L 3N6, Canada. E-mail:joshua.woods@queensu.ca
[3]Professor, Department of Civil Engineering, Queen's University, Ellis Hall, Kingston, ON K7L 5M2, Canada. E-mail: neil.hoult@queensu.ca (corresponding author).
[4]Retired, formerly Senior Manager - Bridge Assessment, Canadian National Railway, 10229 127 Ave. NW, Edmonton, AB T5E 0B9, Canada. Email: Hoat.Le@cn.ca
[5]Bridge Testing Engineer, Canadian National Railway, 17641 Ashland Ave., Homewood, IL 60430, USA. Email: Vamsi.Tolikonda@cn.ca

ABSTRACT

North America's growing demand for rail transportation capacity, both in terms of train weight and length, has raised concerns regarding the performance of older bridges, and has presented the need for improved assessment technologies. A monitoring system composed of discrete and distributed strain sensors combined with a finite element analysis (FEA) may be able to provide critical insights for assessment. One specific area of concern in older railway bridges is their ability to resist longitudinal forces generated by the braking and acceleration of modern diesel-electric engines. To investigate this, two experimental campaigns were undertaken on a steel railway bridge in North Bay, Canada, using data from sensors and an FEA to study longitudinal

force transfer and the impact of rehabilitation with traction bracing. Data from both pre- and post-rehabilitation tests indicated that most axial force in the rail is transferred along its length to a reaction point off the bridge, rather than being transferred immediately into the superstructure. Furthermore, data from the post-rehabilitation tests suggested that the added traction bracing did not significantly affect bridge behavior. Overall, the results demonstrate how field monitoring using conventional and fiber optic strain sensors can be used to assess force transfer between the rail and a superstructure, which could be used as a first step in assessing whether a bridge requires longitudinal strengthening prior to a more comprehensive assessment.

INTRODUCTION

The structural integrity of older railway bridges is becoming an increasing concern to railway companies as they continue to use longer and heavier trains, at faster speeds, to meet growing demands. In fact, 80% of the steel truss bridges owned by Canadian National Railway (CN) predate 1920 (Van Der Kooi *et al*., 2018). Furthermore, it is projected that the volume of interprovincial rail freight tonnage in Canada is expected to increase to 260 million tonnes in 2025, a 30% increase from 2011 (Coed *et al.*, 2016). As a result, between 2005 and 2014, CN and Canadian Pacific Railway invested a combined $1.25 billion annually to maintain, improve, and expand their railway infrastructure (Coed *et al.*, 2016).

There is particular concern surrounding older (i.e. greater than 50 year old) railway bridges' ability to resist the longitudinal forces generated by the braking and acceleration of locomotives (Foutch *et al.*, 2006). Today's diesel-electric engines are capable of generating twice the tractive effort compared to the engines that older bridges were designed for, and thus there exists the possibility that these structures are approaching their capacities (Foutch *et al.*, 2006). Central to assessing these bridges is the need to gain a better understanding of the transfer mechanism of

longitudinal forces between the wheel-rail interface and the bridge superstructure. Although some studies have been conducted on this topic, there is a need to develop monitoring approaches to identify whether this behavior is consistent across a number of bridges. Many railway bridges in Canada are strengthened for longitudinal loads without experimental evaluation, suggesting the possibility that certain bridges are being unnecessarily reinforced or at least over-reinforced. CN currently installs traction bracing at an average cost of $180,000 CAD per span (V. Tolikonda, personal communication, July 8, 2019) to strengthen older bridges against these increasing longitudinal loads (although several factors affect the overall cost of traction bracing installation such as location, scaffolding requirements, span length, permits and labor costs).

If the performance of these bridges can be assessed with greater confidence, critical structures can be prioritized for reinforcement or replacement, which would lead to more efficient spending and greater savings. To accomplish this, better monitoring technologies that are practical to implement and provide accurate information regarding the condition of railway bridges are required. Additionally, the recent development of dynamic distributed fiber optic sensors (DFOS) provides an opportunity to study the distribution of the forces in a way that has never before been possible. DFOS allow the strain to be measured along the length of a member and can be used to assess the behavior of that member under dynamic loads. Previous research has been undertaken to assess the behavior of in-service reinforced concrete structures under static and dynamic loads (Brault et al., Broth and Hoult, 2020), rail bridges under dynamic loads (Van Der Kooi et al., 2018), and even rail tracks under gravity loads (Wheeler et al., 2019). However, this is the first study of its kind to evaluate the use of DFOS for monitoring rails subjected to longitudinal forces due to train passage. Collected monitoring data can be used in conjunction with finite element analysis (FEA) to identify the causes for the observed behavior. To date, only a handful of studies

(e.g. Otter et al., 2001; Srinivas et al., 2013) have sought to monitor the behavior of bridges pre- and post-rehabilitation, and none have used DFOS, so there is a need for more research in this area.

Based on this background, a case study bridge, which was a candidate for rehabilitation with traction bracing to help transfer longitudinal loads, was selected for monitoring with both conventional and distributed strain sensors. Additionally, a 3-D FEA of the bridge was undertaken, prior to rehabilitation, to better understand the observed strain response. The objectives of this case study are to (i) monitor an in-service railway bridge using distributed FOS and strain gauges under various dynamic load cases and compare the results from these sensors, (ii) develop an improved understanding of the longitudinal force transfer in this bridge, (iii) assess the effect of installed traction bracing on the bridge behavior, and (iv) use FEA to evaluate the collected sensor data to and better understand the bridge behavior.

BACKGROUND

Longitudinal Forces in Railway Bridges and the Need for Strengthening

The effects of longitudinal forces on railway bridges needs to be considered in the condition and performance assessment of older structures. A 2010 survey-based study that consulted 16 of North America's foremost experts on railway bridge engineering ranked "longitudinal forces" as the 5th most important research topic for the industry out of a total 22 (Moreu and LaFave, 2012).

Although it is well understood that longitudinal forces originate at the wheel-rail interface due to the effects of rolling friction (Unsworth, 2010), the exact path these loads take through the bridge's various members is less clear. To date, there has been limited research conducted to understand the impact of installing traction bracing on bridge behavior using sensors. A series of

tests was performed to quantify the magnitude of longitudinal forces in several open and ballasted steel deck bridges within the Burlington Northern Santa Fe railroad under the action of locomotive braking and acceleration (Otter *et al.*, 2001). It was found that a maximum longitudinal force occurs while the locomotive is centerd on the bridge and that the longer a bridge segment is, the larger the magnitude of these forces. Furthermore, the measured longitudinal forces were far higher than those predicted by the design guidelines at the time, which led to major revisions to the American Railway Engineering and Maintenance-of-Way Association (AREMA) code, including empirical formulas for calculating tractive force (Otter *el al.*, 2001). A study by Srinivas *et al.* (2013) investigated the longitudinal force transfer mechanism in a single track, steel plate girder bridge in India. A major conclusion from this study was that, during train acceleration tests, 45-65% of the longitudinal force generated in the rail is transferred to the underlying girder (Srinivas *et al.*, 2013). Other researchers (e.g. Al-Emrani et al., 2004) have undertaken numerical studies to evaluate the impact of the placement of traction bracing but have not evaluated their results against field monitoring data. As such, due to the limited number of actual monitoring case studies, there is a need to ensure the conclusions from these studies are applicable across a range of structures.

Rayleigh-Based FOS of Rail Infrastructure

The inclusion of DFOS in rail infrastructure monitoring could offer additional information for use in bridge assessments. For instance, capturing the axial force distribution in rails under train passage requires a high concentration of strain sensors which can be more practically achieved through the use of Rayleigh-based DFOS, which has the unique advantages of small sensor spacing (2.6 mm) and dynamic scanning capabilities (Luna Innovations, 2017), when compared to traditional sensing technologies.

Wheeler *et al.* (2018, 2019) demonstrated that FOS bonded to a rail, with minimal surface preparation, could be used to successfully measure distributed strains. They found that vibration-induced noise exhibited in the data suggested that slower speeds were required to achieve higher accuracy results (Wheeler *et al.*, 2018). This was investigated on an instrumented section of track in Lévis, Quebec, where distributed strain data was measured for freight trains, when speeds were limited to between 8 and 11 km/h (Wheeler *et al.*, 2019). Rayleigh-based DFOS was shown to be a valuable tool for developing an improved understanding of localized rail behavior, which supports the motivation for using such a technology to measure axial force distribution in rails to better understand the transfer of force from the rail to the bridge superstructure.

EXPERIMENTAL METHODS

Test Site

The Newmarket Bridge, pictured in Figure 1 a), is a 4-span steel railway bridge in North Bay, Canada (46°16’6.66” N 79°23’33.70” W). This open-deck, single track structure was designed in 1912 and is made up of three 23 m deck plate girder spans and a single 36 m through plate girder (TPG) span, which was instrumented as part of the current investigation. Each span is simply supported on a series of reinforced concrete piers and abutments, with a fixed joint at its south end and an expansion joint at its north end.

The TPG span at the north end of the bridge was the subject of this research because it was accessible from the ground at the abutment side, allowing for the installation of sensors. The bridge was monitored before and after CN installed traction bracing in bays 1 and 8 of the TPG span for the purpose of improving the structure’s longitudinal force resistance. The member layout and connections for the TPG span before rehabilitation are pictured in Figure 1 b) and Figure 2 shows the structural configuration of the TPG span both before and after the rehabilitation. The track

structure consists of two continuously welded 115 lbs RE rails, with a 1503 mm center-to-center spacing, connected to a series of square wooden ties through an e-clip system. The ties sit directly atop four stringers and are fixed in place using hook bolts, as shown in Figure 2. The stringers are connected to the floor beams through riveted double angle brackets. The diaphragms provide lateral stability for the stringers at their midspan and are connected by single angle riveted brackets. The top flanges of the cross-braces are in direct contact with the bottom flanges of the stringers, which are connected to each other and the main plate girders through built-up plates.

Instrumentation

The monitoring system included both fiber optic sensors and electrical resistance strain gauges. Figure 2 shows the complete sensor layout for both pre- and post-rehabilitation tests and Figure 3 shows a close-up detail of the instrumentation layout in bays 7 and 8 of the TPG span, in which the majority of the sensors were located for both tests due to ease of access. Figure 3 also shows the typical strain gauge positions on the individual member cross-sections.

The fiber optic cable was bonded to the rail at midspan over a 4 m length. As shown in Figure 3, nylon-coated fiber optic sensing cable was installed above and below the assumed neutral axis of the rail at heights of 25 mm and 140 mm, respectively, above the base of the rail. Arranging two cables towards the extreme fibers of the rail allows strains due to both strong-axis bending and axial force to be measured. To install the fiber, the rail was cleaned with a wet rag and a degreasing agent, and the fiber was bonded to the rail using a cyanoacrylate adhesive (Loctite 4851).

To collect DFOS strain measurements, the Luna ODiSI-B was chosen as the fiber optic analyzer because of its high measurement resolution and dynamic sensing capabilities. The

advantages of this system over conventional strain gauges include the ability for up to 20 m of distributed strain sensing at a sampling frequency of 50 Hz, when used in conjunction with a 2.6 mm sensor spacing and 5.2 mm gauge length (Luna Innovations, 2017). However, in this study, only 8 m of fiber (spanning 4 m of rail) was used as previous lab and field results had demonstrated a pattern of poor-quality data in the last 10 m of fiber for this analyzer (Van Der Kooi *et al.*¸ 2018).

To confirm the fiber optic sensor readings and measure the strain in the rail at other locations along the length of the bridge, the rail was instrumented with pairs of strain gauges at locations shown in Figure 2. For the pre-rehabilitation tests, four locations of the rail had strain gauges whereas for the post-rehabilitation tests only two rail locations were instrumented. This was due to the limited number of available sensor channels in the data acquisition system, and the decision to include strain gauges on the newly installed traction bracing during the post-rehabilitation test, which meant some channels from the pre-rehabilitation test needed to be re-allocated. In both campaigns, pairs of strain gauges were bonded to a section of rail past the north end of the TPG span to detect any differences in axial force on and off the bridge. The strain gauges were bonded on the opposite rail to the fiber optic cable to reduce the risk of damaging the fiber during strain gauge installation. Strain gauges (type CEA-06-125UT-350) were bonded at heights of 57 and 95 mm above the base of the rail (see Figure 3), which in a similar way to the DFOS, allowed both axial force and strong-axis bending moments in the rail to be calculated.

In addition to monitoring the strain in the rails, elements of the superstructure were also instrumented with strain gauges (see Figure 3). The midspan of the intermediate floor beam, between bays 7 and 8, had strain gauges installed on the top and bottom flanges of the beam so that the complete 3-D bending profile could be captured under train movement. The floor beams were instrumented due to concern that the stringers could be transferring the longitudinal forces

from the rails into these beams and causing significant out-of-plane bending in these members, which were not designed for this loading. Each of the four cross-braces adjacent to this floor beam were instrumented with a single strain gauge at the vertical neutral axis of its horizontal flange. This was done to minimize the influence of bending effects on the measurements. For the post-rehabilitation tests, both traction braces in bay 8 had a strain gauge installed on the web at the neutral axis and on the bottom flange at the brace midspan to allow for the axial and bending behavior to be investigated. The cross-braces were also instrumented due to concerns that they were being subjected to higher than expected loading. As per the original design intent, the cross-bracing is included to transfer wind loading along the bridge to the abutments and was not designed as traction bracing, and so sensors were installed in an attempt to determine whether or not the members were being unexpectedly loaded.

Test Setup and Procedure

Immediately prior to trains entering onto the bridge, the fiber optic system was zeroed to eliminate all influences of temperature from the data, and data was acquired at 50 Hz. Strain gauge data was recorded automatically and wirelessly at 100 Hz. The strain gauge monitoring system was programmed so that any strain disturbance over a user-specified threshold, representing a train approaching the bridge, would trigger a continuous recording until a specified target channel returned to pre-event strain levels or until a specified time limit was reached. This triggering event also zeroed the gauges so that only the bridge's response to train loads was recorded. The autonomous monitoring capabilities of this system allowed for strain gauge data to be captured for the trains that passed over the bridge at night while the Luna ODiSI-B required manual operation and thus DFOS data could only be collected for trains that passed during the day.

Two separate monitoring campaigns were performed (11 months apart) to investigate the influence of traction bracing on the bridge's behavior. Table 1 summarizes the pre- and post-rehabilitation tests, which included constant velocity, braking, and acceleration tests. The tests were conducted using revenue service freight trains. During braking and acceleration tests, the train decelerated and accelerated, respectively, once the leading locomotive reached the TPG span.

Finite Element Modelling of the Newmarket Bridge

Complementary to the monitoring program, a linear elastic finite element analysis (FEA) of the TPG span (in its pre-rehabilitation state) was developed to validate the collected sensor data and provide additional insights into the behavior of the bridge. The detailed full-scale model, shown in Figure 4, consisted of approximately 1.6 million elements and 2.6 million nodes and was developed using ABAQUS 6.13 (Dassault Systèmes, 2013). The model consists of two built-up plate girders supporting a series of 8 bays that underlie the track system, which was modelled as two continuous rails resting on wooden ties. Each bay consists of two built-up floor beams, four stringers braced by a central diaphragm and a pair of cross-braces, shown in Figure 4 b). All steel parts were assigned an elastic modulus of 210 GPa (Ashby *et al*, 1995) and a Poisson's ratio of 0.3. The wooden ties were assigned a modulus of 12.5 GPa and a Poisson's ratio of 0.35 (Green *et al*, 1999). The model was meshed with standard three dimensional, 8-node linear brick elements and the individual parts were connected using surface-tie constraints, including the connection between the rail to the wooden ties, ignoring the e-clip system. This technique allows for the surfaces of two parts, with different mesh sizes, to be joined together at their nodes. Thus, any pair of surfaces connected in this way will share the same translational and rotational degrees of freedom, which simulates a rigid connection between the two parts (Dassault Systèmes, 2010).

The boundary conditions imposed on the model were chosen to simulate the actual support conditions of the structure, with a pinned bearing at each corner of its south end and a roller bearing at each corner of its north end. Two static load cases were evaluated using the model, shown in Figure 4 c), to evaluate the influence of longitudinal traction forces on the behavior of the bridge. For load case 1, only vertical forces (V) were applied, representing the 6-axle 2951 locomotive, which is a diesel engine with a total mass of 189,000 kg. It was assumed that each wheel applied the same amount of force on the rail and thus a vertical concentrated load of 174 kN was applied to twelve nodes on the head of the rails directly over the instrumented floor beam at the North end of the bridge and spaced longitudinally to match the actual axle spacing (2.007 m). For load case 2, longitudinal forces (L), representing the estimated force due to rolling friction, were included at each of the 12 wheel locations. The magnitude of these forces was taken as 0.3 times the vertical force (= 52 kN), based on the assumed coefficient of friction between a steel wheel and rail (Beagley and Pritchard, 1975; Ertz Knothe, 2002; Ishikawa and Kawamura, 1997).

RESULTS AND DISCUSSION

Distributed vs. Discrete Strain Measurements

The first objective of this research was to monitor an in-service railway bridge under train passage using strain gauges and distributed FOS and assess the feasibility of using FOS to measure the strain distributions in the rail. If distributed strain measurements were possible, they would aid in determining the distribution of axial forces in the rail and the degree to which axial force is transferred between the wheel-rail interface and the bridge superstructure.

To calculate the axial force in the rail using the strain measurements, it is assumed that under loading plane sections remain plane, and that the strain profile varies linearly with height, where the strain at the rail's neutral axis location is the axial strain. Because strain was measured

at two heights along the same section of the rail, as shown in Figure 3 b), the strain at the rail's neutral axis can be determined and the axial force can be calculated as the product of the axial strain, the rail's elastic modulus (207 GPa), and the cross-sectional area (7237 mm^2). When using strains to analyse the member responses in this paper, the assumption of elastic behaviour has been made. It is possible that in a statically indeterminate structure such as this, stresses have become locked in over the years that would invalidate the use of elastic theory to calculate forces and stresses. However, based on the fact that the strains measured during testing under typical train loads were an order of magnitude lower than the anticipated yield strain (~100 microstrain measured maximum values versus ~1250 microstrain for an assumed yield stress of 250 MPa), it was felt that it was unlikely that the members were not behaving elastically. This assumption is also supported by the fact that no unexpectedly high displacements have been noted by the train operator as would be expected for a bridge where the members were behaving inelastically and therefore on the verge of failure.

Figure 5 shows the strains measured above and below the neutral axis by the strain gauges and the DFOS and the calculated axial forces for a single point in time during the pre-rehabilitation braking test. Results are shown at the midspan of the rail for two different train positions: (1) when a train wheel/bogie was within the measurement region, and (2) when a train wheel/bogie was not within the measurement region. It is noted that tensile and compressive strains are positive and negative, respectively. Because the strain gauges were installed at a different height over the rail section depth compared to the DFOS (see Figure 3), the strain gauge data was adjusted, assuming a linear strain profile over the depth of the rail, so that the strain readings were at the same equivalent height on the rail as the DFOS. It is also noted that several localized strain peaks (up to 600 με in magnitude) were observed in the DFOS data, which were the result of vibration-induced

noise, a phenomenon that has been noted in past studies (Van Der Kooi et al., 2018). These points were removed and replaced by linearly interpolating between the closest unfiltered (raw) data points. The filtering algorithm identified the start of a spike based on changes in axial force, between adjacent data points, exceeding a user-defined threshold. A threshold of +/- 2kN was used in this study. To locate the end of a spike, the algorithm found the nearest 26 mm of rail (10 FOS data points) that fell within the threshold.

At the moment in time presented in Figure 5 a), two wheels of a single car bogie moving north (left-to-right in the plot) are located at approximately 2.25 m and 4.25 m along the instrumented rail segment, which generate the two largest spikes in the DFOS strain data. The equal magnitude but opposite sign of the strain measurements from the top and bottom fibers, suggests that locally, rail behavior is dominated by bending rather than by axial force. The distribution of axial force in Figure 5 a) is also not constant along the rail but rather varies with local maximums in compression occurring at the wheel location, which transitions into segments of tension between wheels. However, it is likely that the strain measured at the wheel location falls within a disturbed stress region in the rail, and if so, then the assumptions made in deriving axial force using beam theory would not be appropriate in the immediate vicinity surrounding the wheel locations.

The influence of localized disturbed regions on the rail's axial force distribution can be further investigated by comparing the data in Figure 5 a) to that presented in Figure 5 b), which shows the strain distribution for a point in time, during the same braking test, when the sensors were directly in-between two car bogies (+/- 5.0 m), and thus not directly affected by any axle loads. The results show that when there are no axles immediately over the fiber optic sensor, the distribution of strain, and thus axial force, is relatively uniform through the height of the cross-

306 section and along the entire monitored section of rail, suggesting that indeed it is likely that the
307 strain measured at the wheel location falls within a disturbed stress region. Nonetheless, these
308 results show that the strain gauge and fiber optic data visually agree, which supports the use of
309 distributed sensing for rail strain monitoring, and also demonstrates the advantage that fiber optic
310 sensors have over discrete sensors: the ability to capture the full distribution of strain along the
311 rail, which would be unachievable using strain gauges, as the DFOS data in Figure 5 is displaying
312 roughly 1500 measurements of strain along a 4 m section of rail.

313 ***Pre-Rehabilitation Results***

314 The second objective of this study was to develop an improved understanding of the
315 longitudinal force transfer in this bridge, which can be accomplished by analyzing the distribution
316 of axial forces along the length of the rail and the forces/stresses in the instrumented elements of
317 the bridge superstructure. Figure 6 shows the axial force at the four instrumented locations along
318 34 m of track during the pre-rehabilitation braking test. During this braking test, the train
319 approached the bridge at approximately 30 km/hr, heading north, and applied its brakes once the
320 front-most locomotive reached the TPG span. To indicate the position of the train throughout the
321 test, each subfigure contains a set of vertical dashed lines, labelled with positions 1, 2, and 3 to
322 indicate the point in time that the: (1) front locomotive's first axle entered the TPG span, (2) front
323 locomotive's first axle passed over the strain gauge location for that subfigure, and (3) the train's
324 last axle (after many train cars had passed) cleared the TPG span.

325 The results in Figure 6 show that an axial compressive force is generated almost
326 simultaneously at all four sensor locations due to the locomotive braking prior to reaching the TPG
327 span, which then reaches a maximum when the locomotive crosses over the exact position of the
328 gauges. After reaching the end of the bridge, the train accelerated back to its original speed, which

329 is reflected by the transition of axial force in the rail back into tension as the train accelerates away.
330 The similar behavior among the four rail locations, despite being installed over a 34 m length of
331 track, suggests that axial force introduced at the wheel-rail interface is distributed throughout the
332 length of the rail, and is reacted at a location beyond the measurement locations in this study (i.e.
333 further along the track) rather than being immediately transferred into the bridge superstructure. If
334 the longitudinal axial force were transferred into the bridge superstructure, then each figure would
335 show a jump in axial force only at the moment an axle passes directly over the location of the
336 gauges, followed by an immediate drop back down to zero. The results in Figure 6 also suggest
337 once again that the non-uniform axial force distribution shown in Figure 5 a) is likely due to the
338 sensors closest to the wheel-rail interface being within a disturbed region and that Figure 5 b) likely
339 represents the actual axial force behavior in the rail.

340 Lastly, the net tensile force at the end of the test suggests that the rail shifts under train
341 movement and does not immediately return to its original orientation, a phenomenon that has also
342 been observed by Foutch *et al.* (2006) and Murray *et al.* (2014). Interestingly, the magnitude of
343 the residual axial force along the rail after the train had cleared the bridge (past point 3 in Figure
344 6) gradually increases towards the north end of the bridge, which according to the static analysis
345 of the problem, points towards the existence of an anchorage location (or zone) at the north end of
346 the bridge.

347 The transfer of longitudinal force beyond the north end of the bridge is further examined
348 by comparing the axial force distribution in the rail from the other tests. Figure 7 compares the
349 axial force in the rail at midspan of the TPG during the pre-rehabilitation constant velocity,
350 braking, and acceleration tests. To aid in the explanation of the observed behavior in Figure 7, the
351 force transfer mechanism of a train car applying axial force on a rail with anchorage at its north

end, using the convention given by Unsworth (2010), is also illustrated for each test type. Results in Figure 7 a) show that during the constant velocity test, in the absence of traction forces from braking or accelerating, the rail is in a state of axial compression. In this test, the train was travelling southbound, and thus, if the rail was anchored at its north end, traction forces to maintain the trains velocity would result in axial compression in the rail.

Results in Figure 7 b) show that during the acceleration test, in which the train was travelling northbound, the axial tension force in the rail gradually increases as the train accelerates. This is also in agreement with the force transfer mechanism if the rail was anchored at its north end, as during acceleration the train applies a longitudinal force on the rail in the direction opposite to the direction of motion, resulting in a net axial tensile force.

Finally, results in Figure 7 c) for the braking test show that the response consists of two distinct parts: (1) a braking phase that resulted in axial compression in the rail, and (2) an acceleration phase that resulted in a gradual transition to axial tension in the rail as the train accelerated after clearing the TPG span. The axial tension as the train accelerates away from the bridge in Figure 7 c), which is analogous to the longitudinal force distribution illustrated in Figure 7 b). All of these results point to the existence of an anchorage point at the north end of the bridge, beyond the measurement locations in this study, and suggest that longitudinal force is not transferred to the superstructure of the bridge.

Based on the rail data presented thus far, it would be reasonable to suggest that the behavior of the bridge superstructure should be dominated by vertical loads, rather than longitudinal loads because the strain gauge and FOS data indicate that longitudinal forces were not transferred to the superstructure during the tests. This can be further studied by examining the stress distribution in the instrumented members of the bridge superstructure. If longitudinal force is being transferred

to the superstructure, then there should be some degree of correlation between the axial force generated in the rail and the behavior of the underlying bridge members. Figure 8 compares the axial force generated in the rail at the north end of the TPG span to the response of the floor beam directly under this rail section and the stresses in the adjacent cross braces during the pre-rehabilitation braking test. The floor beam's response, in Figure 8 b), is represented by two curves showing the extreme fiber stress due to bending about the weak axis (the Y-Y axis in Figure 3) on either side of the beam. The extreme fiber stress was calculated by first taking the average of the upper and lower flange strain gauges on the north and south side of the beam (as seen in Figure 3), respectively, as well as the average of all four strain gauges to get the strain at the neutral axis (i.e. the axial strain). The curvature was then calculated as the difference between the north and south average strains divided by the distance between the two sets of gauges (410 mm as seen in Figure 3). The axial strain was removed from the north and south average strains to get the pure bending strains and the curvature was used to extrapolate the strains to the extreme fibers (25 mm from the gauge locations as seen in Figure 3). Finally, the extrapolated strains were multiplied by the Young's modulus (200 GPa) to get the extreme fiber stresses presented in the figure. The results in Figure 8 show that there is no correlation between the axial force in the rail and the stress in the bridge members (floor beam or brace members). The peaks in the stress distribution for the members coincide with individual train wheels/bogies passing over the member locations. These results once again suggest that the axial force generated in the rail is not transferred to the superstructure. Additionally, though the calculated stresses in Figure 8 b) suggest that the floor beams are experiencing out-of-plane bending about the Y-Y axis (see Figure 3), it appears these out-of-plane bending stresses are an order of magnitude lower than the yield stress of the beam, suggesting that they are not likely to cause failure of the beam.

Post-Rehabilitation Results

Following installation of the traction bracing, a second monitoring session was conducted on the TPG span, with sensor locations as shown in Figures 2 and 3. Because the connection between the rail and the superstructure was not altered during rehabilitation, the axial force distribution in the rail under train passage should match the results from pre-rehabilitation tests in terms of general shape and order of magnitude.

Figure 9 shows the axial force in the rail during the post-rehabilitation constant velocity, acceleration, and braking tests for the monitored rail location at the north end of the bridge. The results show a similar pattern of behavior when compared with the pre-rehabilitation test results in Figure 7. In the constant velocity test, the rail is once again in a constant state of compression, the maximum magnitude of which is slightly larger when compared to the pre-rehabilitation test, which is attributed to the higher train velocity (34 km/hr vs. 20 km/hr). The gradual increase in the axial tension in the rail during the acceleration test, shown in Figure 9 b), very closely matches the observed behavior during the pre-rehabilitation test, including a gradual increase in axial tension as the train accelerates. Finally, it is also clear that the action of a locomotive breaking (travelling northwards) induces a compressive axial force in the rail, which transitions into a tensile axial force once the front-most axle passes over the gauges, and which remains in the rail after the full train has cleared the bridge. The maximum axial forces generated in the rail during pre- and post-rehabilitation braking tests also appears to be consistent (ranging between +/- 100 kN).

To monitor the behavior of the newly installed traction braces during the post-rehabilitation tests, strain gauges were installed on the web and the flange of both traction braces at the north end of the bridge. Figure 10 shows the stress calculated at the strain gauge locations on the east and west traction braces, respectively, as well as the out-of-plane bending stresses in the floor

beam during the post-rehabilitation braking test (train travelling northbound). The results show that the neutral axis and bottom flange stresses are similar, suggesting that the traction brace behavior was dominated by axial force and not bending. Furthermore, the results also show the apparent influence that vertical loads have on the traction brace behavior, which shows stress peaks in the data corresponding to individual wheels/bogies passing over the bracing. Based on Figure 10 a) and b), both the east and west traction braces experience similar magnitudes of tensile stress during the passage of a northbound train, which transitions into a net compressive stress once the train clears the span. It was previously demonstrated from strain gauge data on the rail that there is little transfer of longitudinal force into the TPG superstructure for this bridge and this is also confirmed from this data, as there is no correlation between the axial forces generated in the rails and the axial force measured in the traction braces during these tests.

The results in Figure 10 show a correlation between the traction brace behavior and the floor beam's out-of-plane bending, shown in Figure 10 c). Periods when the floor beam's north and south side experience compression and tension, respectively, align with periods of tension in the traction braces. Conversely, when the floor beam's north and south side experience tension and compression, respectively, the traction braces are in compression. This suggests that the axial extension and contraction of the traction braces is a result of the floor beam's tendency to bend out-of-plane, supported by the fact that the flanges of the traction braces connect directly to the web of the floor beams which potentially causes this axial stress.

Comparison of Pre- and Post-Rehabilitation Behavior

This discussion regarding the influence of traction bracing is based on the local behavior of the instrumented superstructure members rather than the whole bridge. For both pre- and post-rehabilitation, the axial force measurements in the rail during constant velocity, acceleration, and

braking tests all have very comparable behaviors and are within the same force ranges. Although the top and bottom flange of both traction braces in bay 8 connect to the web of the instrumented floor beam, there does not appear to be any noticeable differences in the floor beam's behavior before and after rehabilitation. In terms of the braking test data presented, both sets of data show maximum out-of-plane stresses (corresponding to locomotives) of approximately 10-15 MPa.

Based on the pre-rehabilitation test results, which found that there was minimal longitudinal force transfer to the bridge superstructure, it is not surprising that the added traction bracing behaved as it did. It is interesting to note that the rail strain gauge data could be used to determine that there was minimal longitudinal force transfer between the rails and the superstructure, which then could be used as an indicator that the behavior of the structure would be dominated by vertical loading. This lack of force transfer between the rail and the superstructure differs from observations made in previous research (Otter *el al.* 2001; Srinivas *et al.* 2013) and suggests that force transfer can vary from structure to structure. However, results of this work have demonstrated how field monitoring using strain gauges and fiber optic sensors can be used to assess force transfer between the rail and a superstructure. These results could be used as a first step in assessing whether a bridge requires longitudinal strengthening prior to a more comprehensive assessment of the bridge and potentially costly rehabilitation.

Finite Element Modelling Results

As noted earlier, a finite element analysis was conducted to evaluate the sensor data collected during the monitoring study and in an attempt to replicate the behavior of the bridge observed in the field. If it could be shown that the FEA was providing similar results to those observed in the field, it could be used to confirm some of the hypotheses made about the behavior of the bridge, and so the strain results at the location where gauges were bonded (floor beam and

cross-braces) were extracted from the model and compared against the experimental data from the sensors. The FE model and load cases are illustrated in Figure 4. For load cases 1 (vertical loads only) and 2 (vertical loads and longitudinal loads), 12-axle loads, representing the train's leading locomotive during the pre-rehabilitation constant velocity test, were positioned on the rails of the model where the lead axle was directly over the instrumented floor beam and was compared to the same locomotive position from the tests. Table 2 compares the FEA results and field data where the strain gauge locations are labelled in Figure 3.

In general, the finite element results for load case 1 match the strains recorded during the experimental study with reasonable accuracy. The combination of floor beam strains suggests that this member is experiencing bi-axial bending, in the same way that was hypothesized during the discussion of the experimental results. Although the strains from the finite element model at SG3 and SG4 do not match the measured strains with the same degree of accuracy as SG1 and SG2, they still show that the north side of the beam is being strained more than the south side (i.e. there is weak axis bending). The finite element results for the cross-braces reflects the same pattern of strain measured by the gauges, with the exception of SG5.

With the exception of SG5, all finite element results for load case 1 demonstrate errors of less than 45%, with minimum errors of 1.4% and 2.2% from SG1 and SG2, respectively. Possible reasons for high errors lie in the assumptions made when developing the model. For example, the surface-tie constraints made between each part may overestimate the stiffness of the connections between bridge members which, in reality, were connected by rivets. Furthermore, it was assumed that the wooden ties were isotropic and elastic, when in reality they would exhibit nonlinear orthotropic behavior. It is also possible that the exact support conditions assigned to the model do not perfectly reflect the behavior of the bridge bearings. The model also represents a geometrically

perfect idealization of the actual structure and thus does not incorporate deterioration or wear that may have been experienced by the bridge in its over 100-year lifespan. Additionally, it was assumed that each axle applies the exact same static vertical load to the bridge, which may not be entirely accurate depending on the weight distribution of the actual locomotive and ignores any dynamic effects during field testing. However, the general behavior of the model under load case 1 appears to reflect the response of the actual bridge, which confirms the experimental hypothesis that vertical forces dominate the overall bridge response rather than any longitudinal forces that may be present at the wheel-rail interface.

This notion is supported further by the increased percent errors for all locations under load case 2, which included longitudinal loads. Although the magnitude of the applied longitudinal force was based on an assumed coefficient of friction between the wheels and rail, the FEA results show that the addition of the traction force causes the results to deviate from the observed behavior in the field, and thus any variation in the applied longitudinal force is not expected to produce results that are in better agreement with the collected data. These results once again suggest that a first step in assessing whether a bridge requires rehabilitation for longitudinal loads could include a combination of field monitoring coupled with FEA, which can help to validate collected data and be used for additional bridge performance assessment if required (e.g. estimating deflections) prior to investing in costly bridge rehabilitation.

CONCLUSIONS

This research case study explored the use of distributed fiber optic sensors in railway bridge monitoring as a complimentary technology to discrete strain gauges to investigate the performance of a bridge before and after traction bracing was installed. Both pre- and post-rehabilitation tests were conducted on the TPG span of the Newmarket Bridge: a 4-span, single track steel plate girder

structure located in North Bay, Canada. For both sets of tests, strains in the rail and various superstructure members were measured as freight trains performed acceleration, braking, and constant velocity tests over the TPG span. To assist with the structural analysis of the bridge, a full-scale, three-dimensional finite element model of the Newmarket Bridge's TPG span was developed. Two static load cases, simulating vertical and longitudinal forces from the leading locomotive were applied to the model. Key conclusions from the research are as follows:

- The visual agreement between distributed and discrete strain data supports the use of DFOS as a tool for capturing distributed rail behavior under train passage.
- For the Newmarket Bridge, the simultaneous development of axial force along 34 m of rail under train movement suggests that there is minimal longitudinal force transfer into the superstructure. This result is different from previous research and suggests that the transfer of longitudinal force from the rail to the superstructure can vary from bridge to bridge.
- The instrumented floor beam demonstrates bi-axial bending behavior at its midspan, which does not appear to be mitigated by the addition of traction bracing in the adjacent bay. The traction braces in bay 8 of the TPG span demonstrate a mostly axial response to train passage, which appears to correlate with the floor beam's out-of-plane bending behavior.
- The floor beam, cross-brace, and traction brace behavior appears to be dominated by the effects of vertical train loads, which reinforces the notion that the bridge resists minimal longitudinal force.
- The data suggests that an initial sensor installation of strain gauges or FOS on the rail both on and off the bridge could indicate whether there is longitudinal force transfer between the rail and the superstructure, and thus whether further monitoring and/or rehabilitation is required.

- Comparison between the finite element analysis and the experimental results confirms that the bridge response is dominated by vertical loads, rather than longitudinal.
- The braking forces produced by the test trains were potentially limited due to the fact that the trains did not engage their emergency brakes and so future tests could examine the impacts of the higher braking forces although further safety considerations would be required.

DATA AVAILABILITY STATEMENT

All data, models, and code that support the findings of this study are available from the corresponding author upon reasonable request.

ACKNOWLEDGEMENTS

The authors are grateful to the Natural Sciences and Engineering Council of Canada and Canadian National Railway for financial support of this research. For their valuable technical assistance in executing the field monitoring trips, the authors would like to thank Jefferey Jones of Canadian National Railway in addition to Jacob Yager, Simon Howell, and Ryan Collison of Queen's University.

REFERENCES

Al-Emrani, M., Åkesson, B., & Kliger, R. (2004). Overlooked secondary effects in open-deck truss bridges. Structural engineering international, 14(4), 307-312.

American Railway Engineering and Maintenance-of-Way Association (AREMA). (2018). Chapter 15 Steel Structures. *AREMA 2018*. Washington, D.C.

556 Ashby, M.F., Gibson, L.J., Wegst, U., and Olive, R. (1995). The mechanical properties of natural
557 materials. I. material property charts. *Proc. R. Soc. Lond. A. 450,* 123-140.
558 https://doi.org/10.1098/rspa.1995.0075
559 Beagley, T.M., and Pritchard, C. (1975). Wheel/rail adhesion – the overriding influence of water.
560 *Wear, 35*(2), 299-313. https://doi.org/10.1016/0043-1648(75)90078-2
561 Brault, A., Hoult, N. A., Greenough, T., & Trudeau, I. (2019). Monitoring of beams in an RC
562 building during a load test using distributed sensors. Journal of Performance of
563 Constructed Facilities, 33(1), 04018096.
564 Broth, Z. E., & Hoult, N. A. (2020). Field Monitoring of RC-Structures under Dynamic Loading
565 Using Distributed Fiber-Optic Sensors. Journal of Performance of Constructed Facilities,
566 34(4), 04020070.
567 Coed, L., Knowles, J., Lauerman, V., Robins, A., and Gill, V. (2016). *Building for Growth:*
568 *Trade, Rail, and Related Infrastructure* [Research Report]. Retrieved on April 9, 2019
569 from The Conference Board of Canada website:
570 https://www.conferenceboard.ca/temp/ca296e17-8ded-498e-bc83-
571 1707201b1ea7/7722_Building_Growth_Trade_Rail_Infrascture_RPT_FR.pdf
572 Dassault Systèmes. (2010). *Abaqus/CAE User's Manual (6.10)* [User Guide]. Retrieved on
573 August 17, 2019 from
574 https://www.sharcnet.ca/Software/Abaqus610/Documentation/docs/v6.10/books/usi/defa
575 ult.htm
576 Ertz, M., and Knothe, K. (2003). Thermal stresses and shakedown in wheel/rail contact. *Archive*
577 *of Applied Mechanics, 72*(10), 715-729. https://doi.org/10.1007/s00419-002-0255-4

578 Foutch, D.A., Kim, T.W., Otter, D.E., and Doe, B.E. (2006). Investigation of longitudinal forces
579 in a concrete railroad trestle. *Journal of Bridge Engineering, 11*(5), 618-625.
580 https://doi.org/10.1061/(ASCE)1084-0702(2006)11:5(618)
581 Green, D.W., Winandy, J.E., and Kretschmann, D.E. (1999). Chapter 4 Mechanical Properties of
582 Wood. *Wood handbook – Wood as an engineering material.* Gen. Tech. Rep. FPL–GTR–
583 113. Madison, WI: U.S. Department of Agriculture, Forest Service, Forest Products
584 Laboratory. Retrieved from https://www.fpl.fs.fed.us/documnts/fplgtr/fplgtr113/ch04.pdf
585 Ishikawa, Y., and Kawamura, A. (1997). Maximum adhesive force control in super high speed
586 train. *Proceedings of Power Conversion Conference – PCC '97, 2*, 951-954.
587 https://doi.org/10.1109/PCCON.1997.638382
588 Luna Innovations. (2017). *ODiSI-B Data Sheet*. Retrieved from https://lunainc.com/wp-
589 content/uploads/2016/07/ODB5_DataSheet_Rev13_020217.pdf
590 Moreu, F., and LaFave, J.M. (2012). *Current research topics: railroad bridges and structural*
591 *engineering* (Report No. NSEL-032). Retrieved from Illinois Digital Environment for
592 Access to Learning and Scholarship website:
593 https://www.ideals.illinois.edu/bitstream/handle/2142/34749/NSEL%20Report%20More
594 u-Lafave.pdf?sequence=2&isAllowed=y
595 Murray, C.A., Take, A.W., and Hoult, N.A. (2014). Measurement of vertical and longitudinal
596 rail displacements using digital image correlation. *Canadian Geotechnical Journal, 52*,
597 141-155. https://doi.org/10.1139/cgj-2013-0403
598 Otter, D.E., LoPresti, J.A., and Sweeney, R.A.P. (2001). Longitudinal forces in bridges due to
599 heavy haul freight operations. *7th International Heavy Haul Conference*. International
600 Heavy Haul Association, Virginia Bach, Va., 565-568. Retrieved from

http://railknowledgebank.com/Presto/content/GetDoc.axd?ctID=MTk4MTRjNDUtNWQ0My00OTBmLTllYWUtZWFjM2U2OTE0ZDY3&rID=MTY4MQ==&pID=Nzkx&attchmnt=True&uSesDM=False&rIdx=MjI3Nw==&rCFU=

Srinivas, V., Ramanjaneyulu, K., Kumar, K.S., Parivallal, S., Kesavan. K, Ravisankar, K., Lakshmanan, N., and Iyer, N.R. (2013). Evaluation of longitudinal force on a railway bridge based on strain measurements. *Experimental Techniques 37*(1), 55-67. https://doi.org/10.1111/j.1747-1567.2011.00747.x

Unsworth, J.F. (2010). *Design of Modern Steel Railway Bridges.* CRC Press. Boca Raton, FL, USA.

Van Der Kooi, K., Hoult, N.A., and Le, H. (2018). Monitoring an in-service railway bridge with a distributed fiber optic strain sensing system. *Journal of Bridge Engineering, 23*(10), 05018007. https://doi.org/10.1061/(ASCE)BE.1943-5592.0001281

Wheeler, L.N., Pannese, E., Hoult, N.A., Take, W.A., and Le, H. (2018). Measurement of distributed dynamic rail strains using a Rayleigh backscatter based fiber optic sensor: Lab and field evaluation. *Transportation Geotechnics, 14*(1), 70-80. https://doi.org/10.1016/j.trgeo.2017.10.002

Wheeler, L.N., Take, W.A., Hoult, N.A., and Le, H. (2019). Use of fiber optic sensing to measure distributed rail strains and determine rail seat forces under a moving train. *Canadian Geotechnical Journal*, *56*(1), 1-13. https://doi.org/10.1139/cgj-2017-0163

Tables

Table 1: Summary of pre- and post-rehabilitation tests

Bridge Condition	Test Type	Time of Day	Direction of Travel	Approximate Speed[a] (km/hr)
Pre-rehabilitation	Acceleration	Day	North	8
	Constant Velocity	Night	South	20
	Braking	Day	North	30
Post-rehabilitation	Acceleration	Day	North	10
	Constant Velocity	Night	South	34
	Braking	Day	North	24

[a] Approximate approach speeds prior to initiation of braking/acceleration at TPG span.

Table 2: Comparison of experimental and finite element results for static load cases.

			Load Case 1 (Vertical Loading only)		Load Case 2 (Vertical + Longitudinal)	
Strain Gauge (SG)[a]	Location on Bridge	Experimental Result (με)	Finite Element Result (με)	Percent Error (%)	Finite Element Result (με)	Percent Error (%)
SG1	Floor Beam Top + North	-207	-210	1.4	-184	11.1
SG2	Floor Beam Top + South	-89	-87	2.2	-122	37.1
SG3	Floor Beam Bot. + North	95	138	45.3	157	65.3
SG4	Floor Beam Bot. + South	200	145	27.5	134	33.0
SG5	Bay 8 East Brace	-5	18	260	29	480.0
SG6	Bay 8 West Brace	9	7.1	21.1	49	444.4

[a] Figure 3 shows the locations of strain gauges 1 – 6 on the pre-rehabilitated bridge components

List of Figure captions

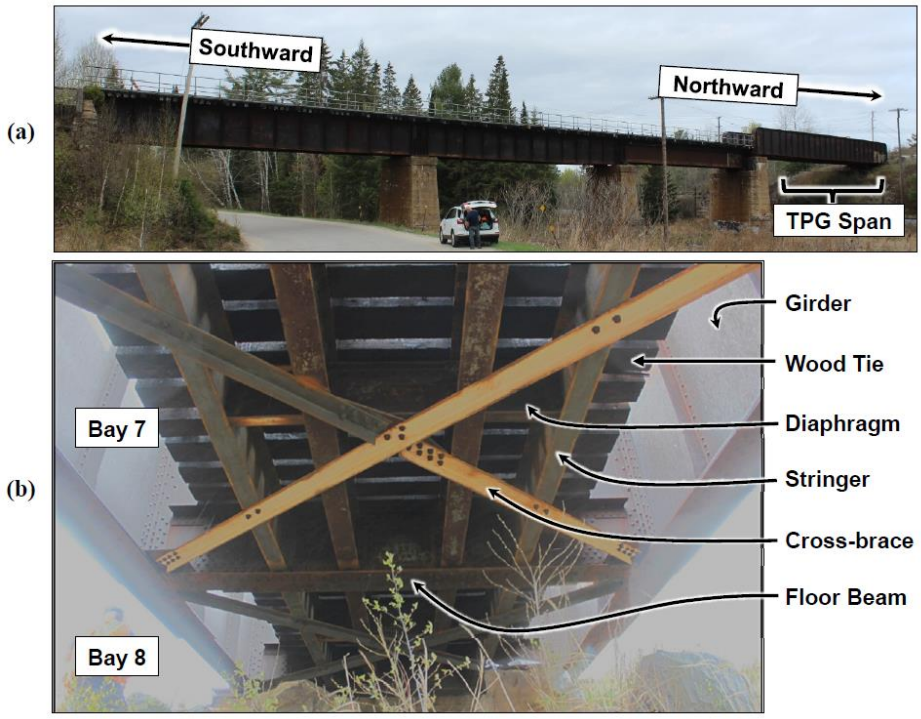

Figure 1: a) The Newmarket Bridge and b) Bay's 7 and 8 of the TPG span (pre-rehabilitation).

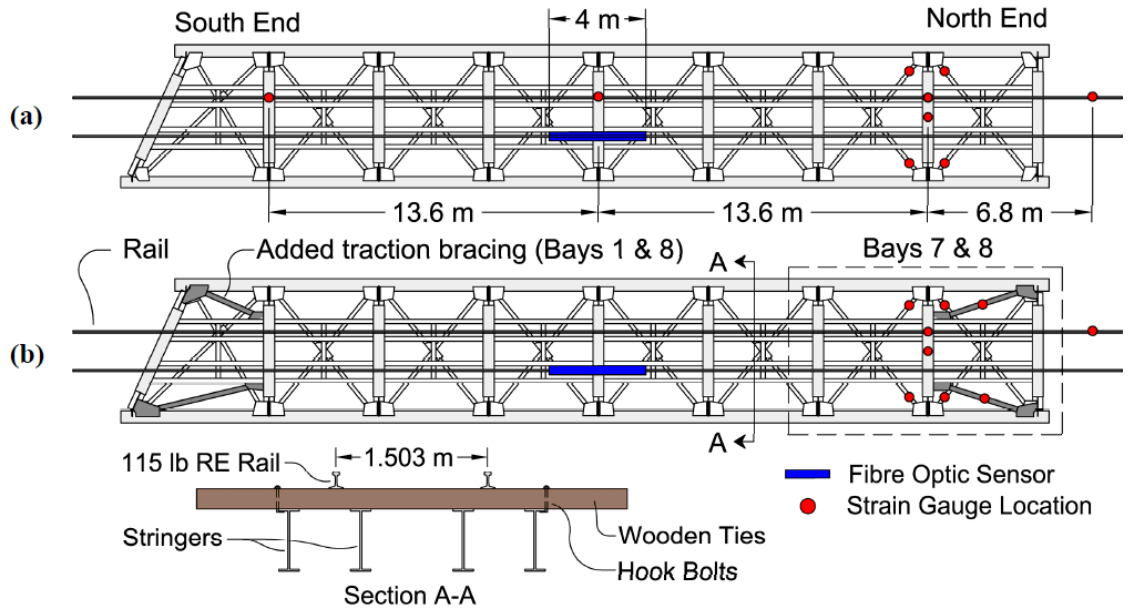

Figure 2: Bridge configuration and sensor layout: (a) Pre-rehabilitation, (b) Post-rehabilitation.

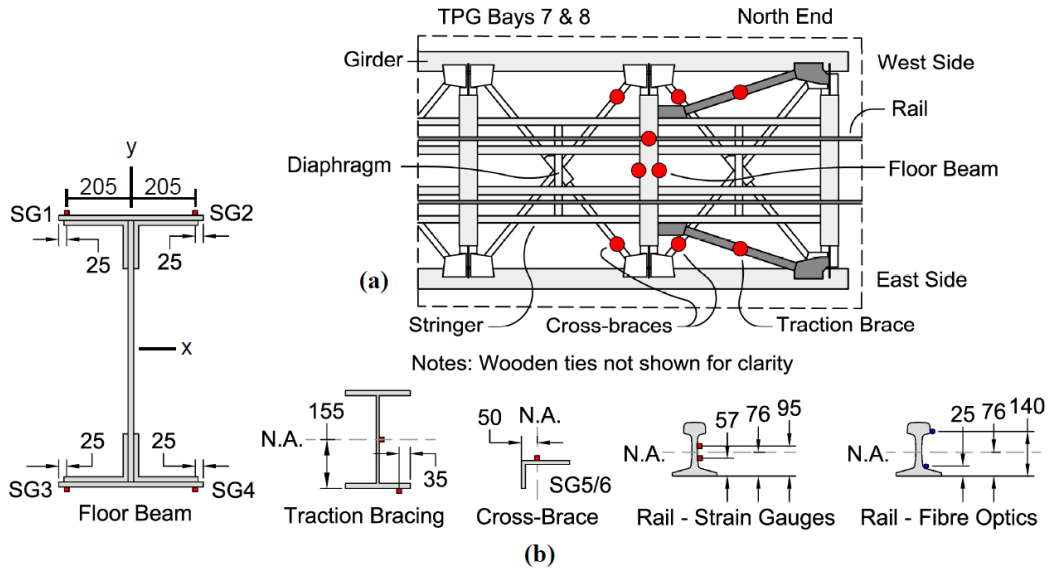

634

635 Figure 3: Instrumentation layout: (a) TPG Bays 7 and 8, (b) Cross-section details (units: mm)

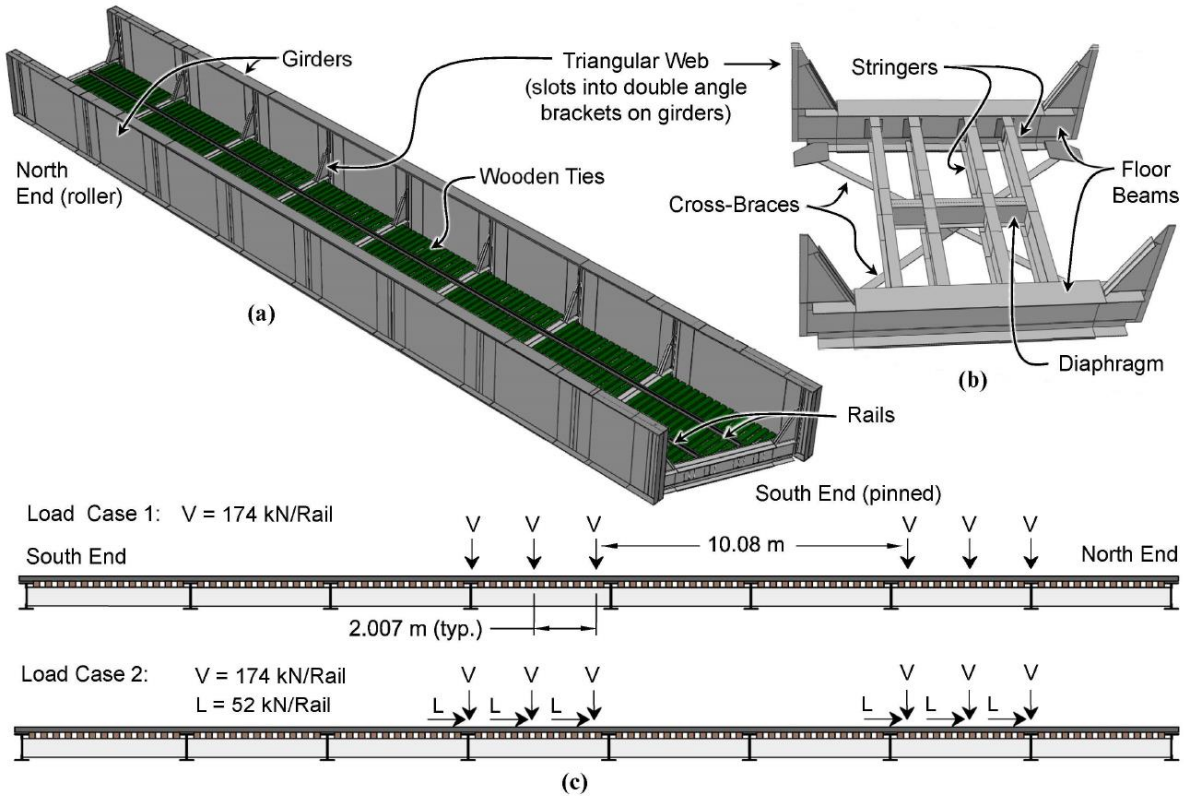

636

637 Figure 4: Finite element model of the bridge: (a) TPG span, (b) Typical Bay (c) Load cases

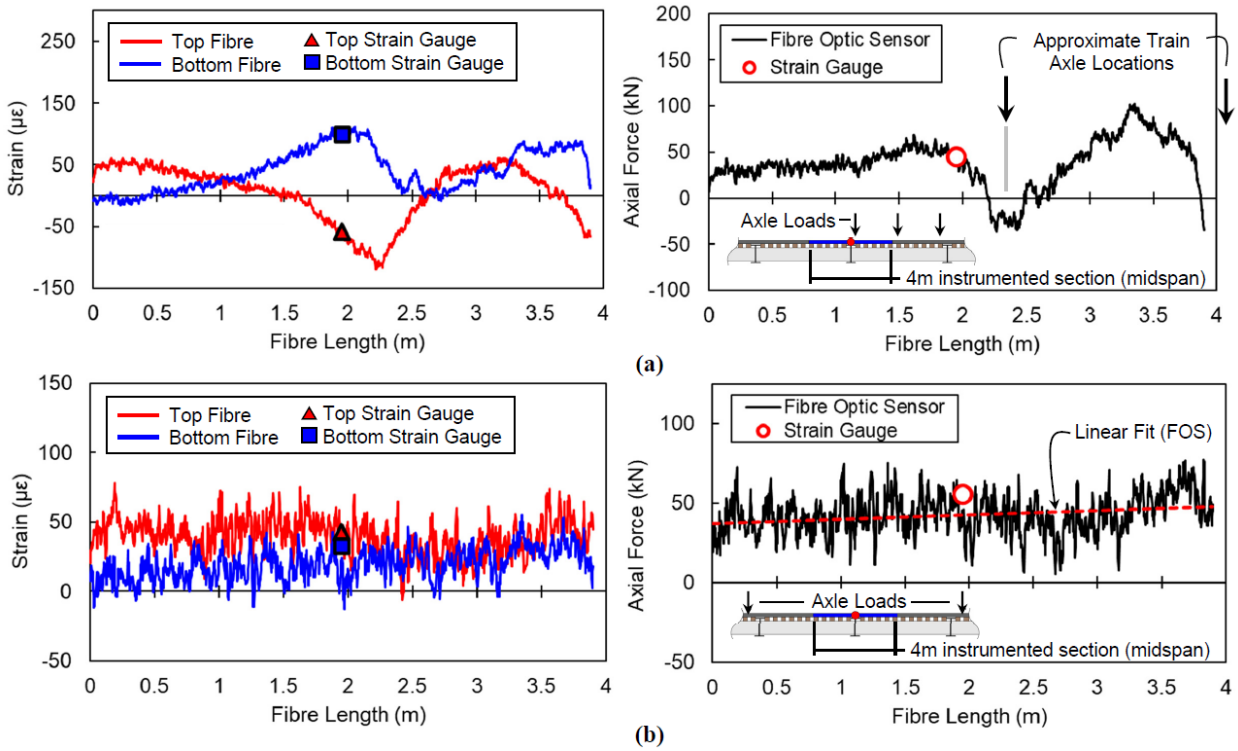

638

639 Figure 5: Comparison of strain (left) and axial force (right) at the TPG midspan for the pre-
640 rehabilitation braking test: (a) bogie in measurement region, (b) bogie outside measurement
641 region.

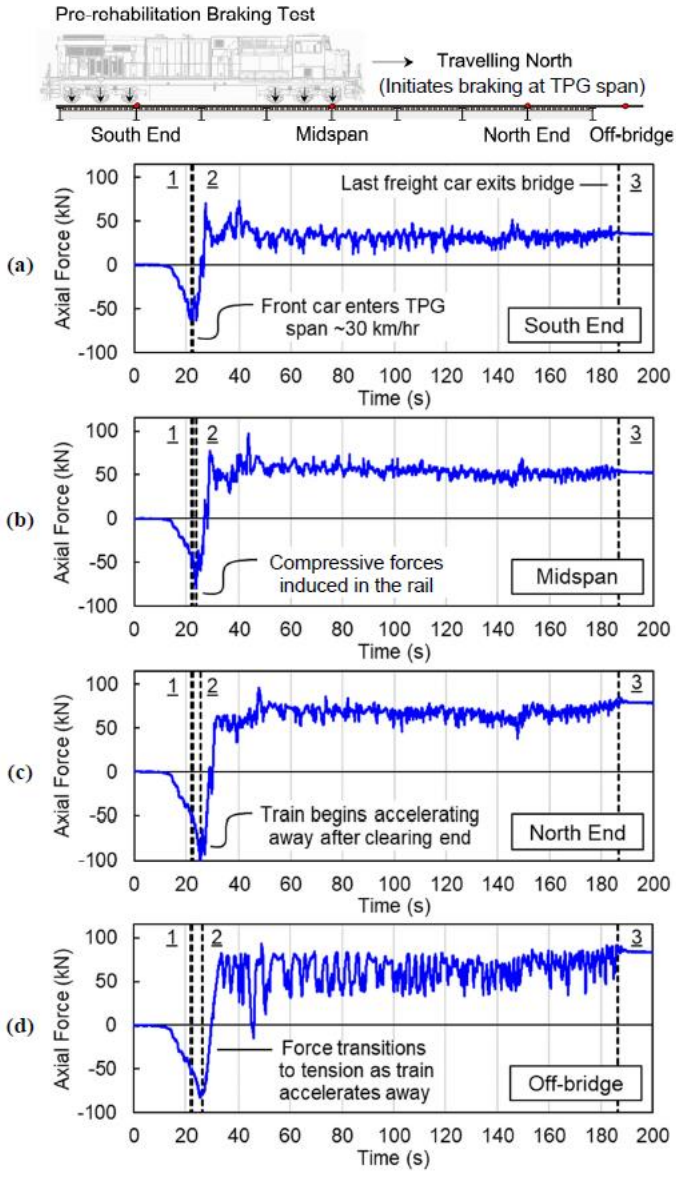

642

643 Figure 6: Axial force in the rail at the a) South end, b) Midspan, c) North end, and d) Off-bridge

644 sensor locations during the pre-rehabilitation braking test.

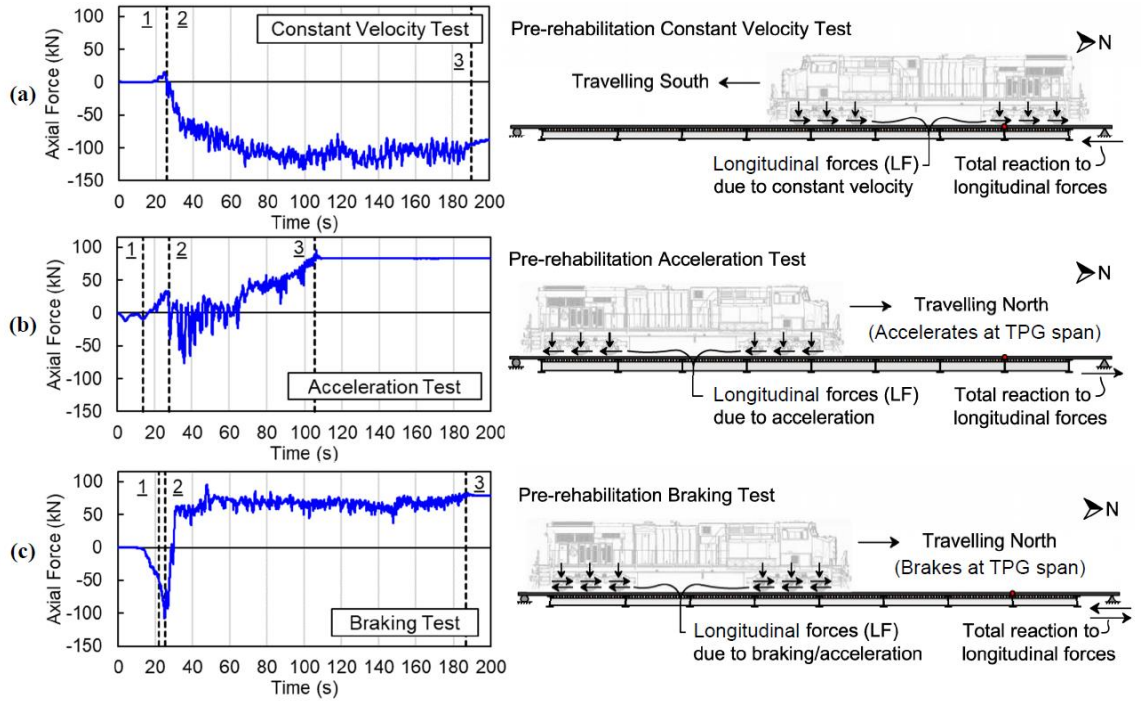

645

646 Figure 7: Axial force in the rail at the north end of the bridge during the pre-rehabilitation

647 a) constant velocity test, b) acceleration test, c) braking test.

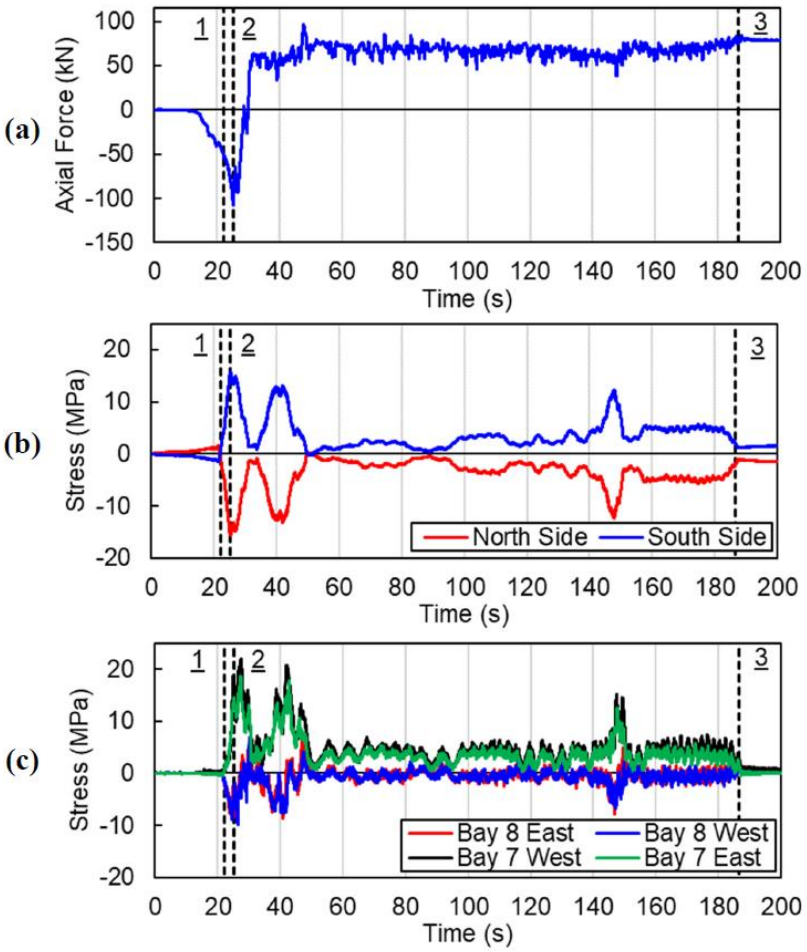

Figure 8: a) Axial force in the rail at the north end location, b) out-of-plane bending stress in the floor beam, and c) cross-brace stress during the pre-rehabilitation braking test.

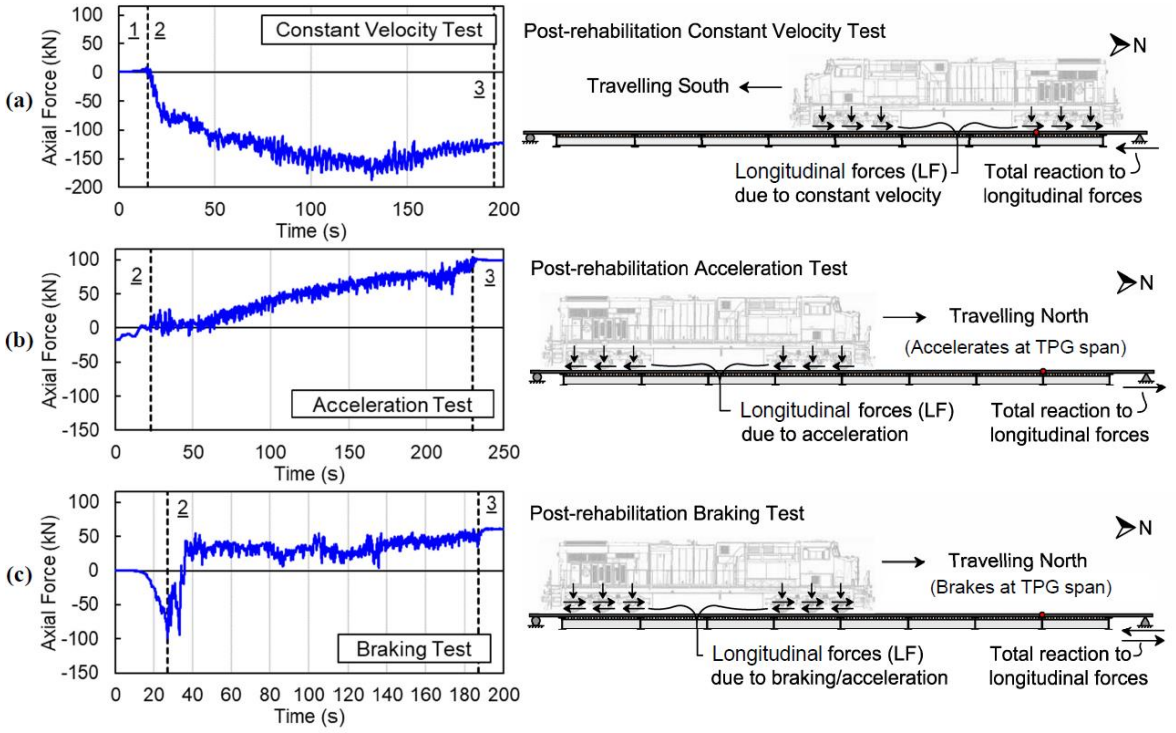

Figure 9: Axial force in the rail at the north end of the bridge during the post-rehabilitation tests: a) Constant velocity test, b) Acceleration test, c) Braking test.

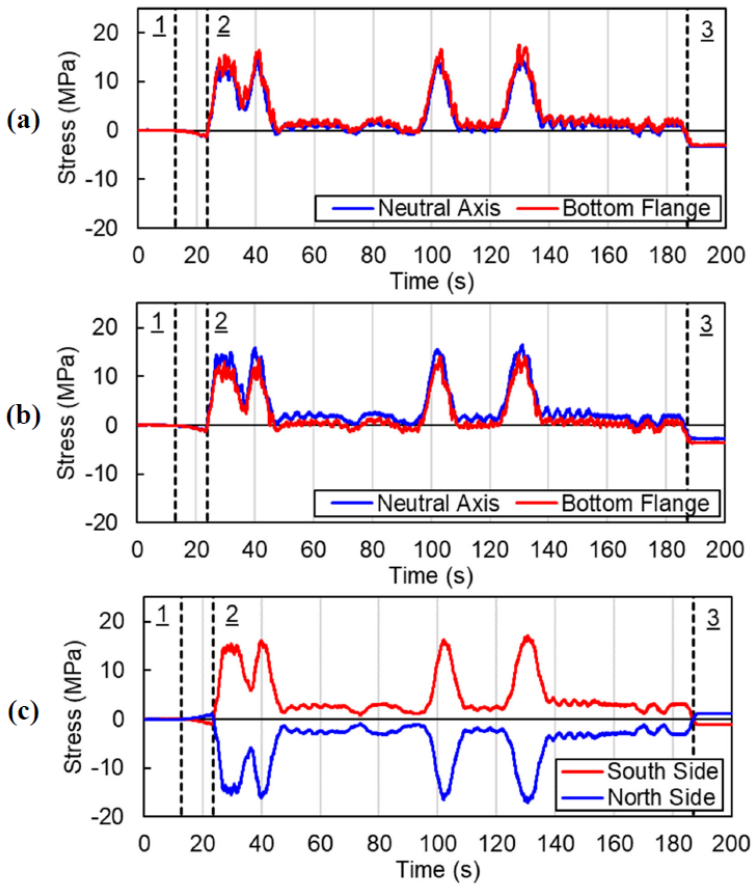

654

655 Figure 10: Stress with time of the a) east traction brace and b) west traction brace compared to

656 the c) out-of-plane bending stress in the floor beam during post-rehabilitation braking test 1.